

Article

Optimization of High-Alumina Blast Furnace Slag Based on Exergy Analysis

Zhen Wang ¹ , Haiyan Zheng ^{1,2,*} , Yan Zhang ¹ and Liang Ge ¹

¹ School of Metallurgy, Northeastern University, Shenyang 110819, China; 2210654@stu.neu.edu.cn (Z.W.); 2071658@stu.neu.edu.cn (Y.Z.); gl1793307551@163.com (L.G.)

² Key Laboratory for Ecological Metallurgy of Multimetallurgical Mineral (Ministry of Education), Northeastern University, Shenyang 110819, China

* Correspondence: zhenghy@smm.neu.edu.cn

Abstract: Raw material with a high Al_2O_3 content has led to an increase in the Al_2O_3 content in blast furnace slag, which has affected the normal operation of a blast furnace. The exergy analysis method is an important method for studying the energy utilization of high-alumina blast furnace smelting. In this paper, to investigate the impact of slag composition on exergy efficiency and optimize exergy efficiency during the smelting process of high Al_2O_3 iron ore, a gray box exergy analysis model of blast furnace smelting and an objective function for minimizing the total exergy loss were developed. The results indicated that the blast furnace smelting process had an exergy efficiency (η) of 28.29% for hot metal and slag; the exergy efficiency of the blast furnace did not significantly increase with the increasing $w(\text{MgO})/w(\text{Al}_2\text{O}_3)$ and R ($w(\text{CaO})/w(\text{SiO}_2)$), but the exergy efficiency of the blast furnace declined with increasing $w(\text{Al}_2\text{O}_3)$. The regional optimal solution for the objective function method was 7129.42 MJ with slag compositions of $R = 1.295$, $w(\text{MgO})/w(\text{Al}_2\text{O}_3) = 0.545$, and $w(\text{Al}_2\text{O}_3) = 15\%$.

Keywords: blast furnace ironmaking; exergy analysis; slag optimization; objective function; high-alumina blast furnace slag



Citation: Wang, Z.; Zheng, H.; Zhang, Y.; Ge, L. Optimization of High-Alumina Blast Furnace Slag Based on Exergy Analysis. *Metals* **2024**, *14*, 465. <https://doi.org/10.3390/met14040465>

Academic Editor: Henrik Saxen

Received: 15 March 2024

Revised: 9 April 2024

Accepted: 10 April 2024

Published: 15 April 2024



Copyright: © 2024 by the authors. Licensee MDPI, Basel, Switzerland. This article is an open access article distributed under the terms and conditions of the Creative Commons Attribution (CC BY) license (<https://creativecommons.org/licenses/by/4.0/>).

1. Introduction

China has progressively increased its imports of iron ore in recent years, with 61.65% of imports originating from Australia (2021) [1,2]. Australian ores have a high $w(\text{Al}_2\text{O}_3)$ content ($w(\text{Al}_2\text{O}_3)$), which results in a high $w(\text{Al}_2\text{O}_3)$ in the blast furnace smelting process [3–12]. The operation of the blast furnace is impacted, and the quality of the hot metal is reduced due to the high $w(\text{Al}_2\text{O}_3)$ content in the smelting process [13,14]. In addition, the energy used by China's steel industry was shown to constitute approximately 11% of the country's total energy consumption, and the energy used by the blast furnace smelting process constituted approximately 59% of that total by 2022. Therefore, reducing energy consumption in the blast furnace smelting process has emerged as a key strategy for achieving energy conservation and consumption reduction in Chinese iron production [15–17].

The exergy analysis method, which is more objective and thorough than conventional energy use theories, can evaluate energy in terms of its amount and quality. Exergy analysis was first used in the metallurgical industry by Szargut J. [18]. Brauer H. et al. applied the exergy analysis method to the thermodynamic study of the blast furnace smelting process, analyzing the efficiency of the smelting process and providing methods for energy conservation and consumption reduction in the entire steel industry [19]. Akiyama et al. used exergy analysis methods to evaluate the energy usage in direct reduction-electric furnace, smelting reduction, and blast furnace smelting processes [20–22]. Computational research on boiler heat balance and exergy balance was established by Liu et al. [23]. A mass balance and an exergy balance for ladle refining (LF) were created by Min et al. using the exergy analysis method to analyze the energy utilized throughout the refining process in an LF furnace [24]. Exergy flow analysis was devised by Zhang et al. at the process and system

levels [25]. To investigate the effects of adding iron coke on the material consumption and energy usage efficiency of blast furnaces, Guo et al. [26] developed an exergy balance model for the use of iron coke in blast furnaces. After adding iron coke, the indirect reduction degree in the furnace is increased, the carbon utilization rate is improved, and the carbon consumption and slag amount per unit of hot metal in smelting are reduced. Qiu et al. [27] established a material and energy optimization model including intermolecular chemical reactions and analyzed the direct reduction process of a hydrogen metallurgical shaft furnace. The gas-based shaft furnace was optimized with the goal of increasing the gas utilization ratio, and the optimized intensity was reduced by 8796.43 MJ/t. Sun et al. [28] found that the intensity and exergy loss of the iron and steel industrial production processes were the focus of the study. The flue gas of coking and sintering caused a large amount of exergy loss, which was 233.887 MJ/t and 182.233 MJ/t, respectively, accounting for 15.32% and 8.79% of the total exergy loss of the corresponding process.

The structure of the blast furnace burden affects the smooth operation of blast furnace smelting and the quality of the final products. However, due to the complex changes in burden structure, slag compositions with relatively small changes were taken as the variables to explore the changes in the overall efficiency of blast furnace smelting. In this paper, an exergy analysis model for blast furnace smelting with high Al_2O_3 content iron ore was established. The transmission and conversion of exergy flow during the smelting process of a high-alumina blast furnace were analyzed, and the effects of the slag composition (the ratio of basicity (R , $w(\text{CaO})/w(\text{SiO}_2)$), $w(\text{MgO})/w(\text{Al}_2\text{O}_3)$), and $w(\text{Al}_2\text{O}_3)$) on the furnace's total exergy efficiency were discussed. Additionally, an objective function was established based on the gray box exergy analysis model with the goal of decreasing exergy loss to find a suitable slag composition. This study provides a theoretical basis for the changes in the burden structure, energy conservation, and consumption reduction of the blast furnace during the smelting process.

2. Establishment of an Exergy Analysis Model for Blast Furnace Smelting

2.1. Exergy Analysis Model

In this study, an exergy analysis of a blast furnace was conducted by using the Chinese national standard GB/T 14909-2021 "Technical Guidelines for Exergy Analysis of Energy Systems" [29].

There are three types of exergy analysis models: the black box exergy analysis model, the gray box exergy analysis model, and the white box exergy analysis model. A comparison of their characteristics is shown in Table 1. As shown in Table 1, the gray box exergy analysis model is an analysis model that lies between the black box and white box exergy analysis models. This model avoids the simple analysis of system energy consumption by the black box exergy analysis model, and its calculation process and data acquisition are relatively simple compared to those of the white box exergy analysis model. Therefore, considering all factors, the gray box exergy analysis model was selected to analyze the overall energy consumption of the blast furnace in this study.

The gray box exergy analysis model for blast furnace smelting in this study is shown in Figure 1. The exergy input in the blast furnace includes the chemical exergy of the fuel (coke and coal), the exergy of the blast (the chemical exergy of the blast and the physical exergy of the blast), the chemical exergy of the ore (sinter, pellet, and lump ore), and the chemical exergy of the flux. The internal exergy losses (i.e., process losses) include the exergy loss of chemical reactions, the exergy loss of heat transfer, the exergy loss of gas pressure, and the mixing process. The exergy of the product (hot metal and slag) and the external exergy losses (such as the exergy of gas, the exergy lost during furnace dust, and other exergy losses) are components of the output. The exergy input is equal to the sum of the process loss and exergy output.

Table 1. The characteristics of the three exergy analysis models.

Exergy Analysis Model	Implication	Characteristics		
		Calculate Complexity	Analysis Accuracy	Data Acquisition
Black box exergy analysis model	The structure of the model is simple: macro-analysis system energy consumption.	Simple	Fuzzy	Easy to obtain, but not accurate
Gray box exergy analysis model	An analysis model between the black box analysis model and the white box analysis model, which can analyze the system energy consumption in detail.	Relatively complex	Relatively accurate	Easy to obtain and relatively accurate
White box exergy analysis model	The structure is complex, and the energy consumption of each part in the system is analyzed in detail.	Complex	Accurate	Difficulty in obtaining

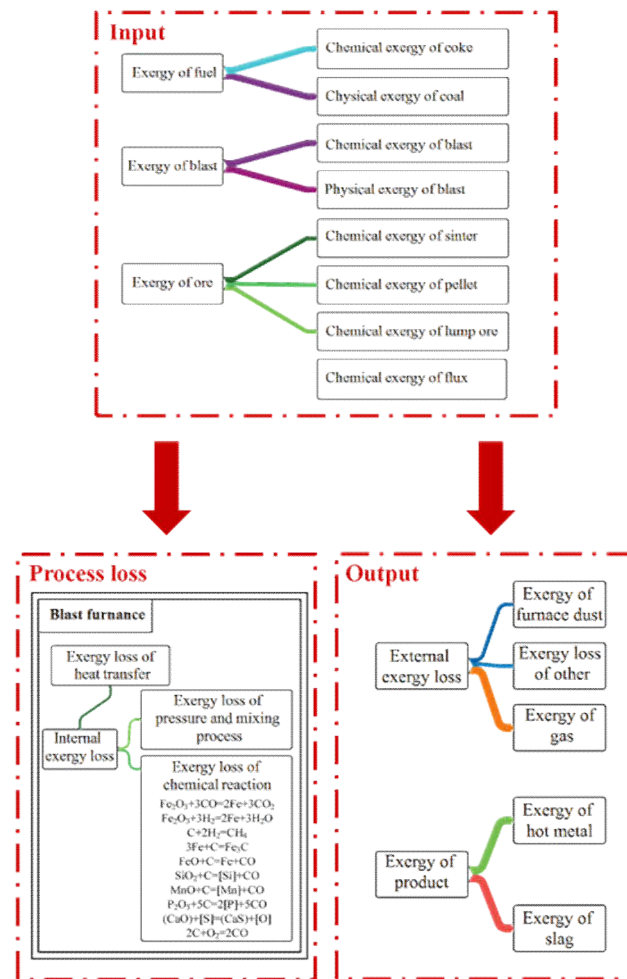


Figure 1. Exergy analysis model diagram of blast furnace smelting.

The calculation method for the exergy value involved in the gray box exergy analysis model is shown in Table 2. The definitions of the symbols in Table 2 are shown in Table 3.

Table 2. Calculation method of exergy.

	Calculation Method	No.
Chemical exergy of fuel (MJ)	$E_{x, \text{ch, fuel}} = m_{\text{fuel}}(Q_{\text{low}} + rw)$	(1)
Physical exergy of blast (MJ)	$E_{x, \text{ph, blast}} = m_{\text{blast}} \left(c_{p_{\text{blast}}} (T_{\text{blast}} - T_0) - c_{p_{\text{blast}}} T_0 \ln \left(\frac{T_{\text{blast}}}{T_0} \right) \right) + \frac{1}{2} m_{\text{blast}} v_{\text{blast}}^2 + n_{\text{blast}} R_0 T_0 \ln \left(\frac{p_{\text{blast}}}{p_0} \right) \times 10^{-3}$	(2)
Chemical exergy of blast (MJ)	$E_{x, \text{ch, blast}} = \sum x_{\text{blast}, i} E_{x, \text{ch, blast}, i} + R_0 T_0 \sum x_{\text{blast}, i} \ln(x_{\text{blast}, i})$	(3)
Chemical exergy of iron ore (MJ)	$E_{x, \text{ch, iron ore}} = \sum x_{\text{iron ore}, i} E_{x, \text{ch, iron ore}, i}$	(4)
Chemical exergy of flux (MJ)	$E_{x, \text{ch, flux}} = \sum x_{\text{flux}, i} E_{x, \text{ch, flux}, i}$	(5)
Physical exergy of hot metal (MJ)	$E_{x, \text{HM}} = m_{\text{HM}} \left(c_{p_{\text{HM}}} (T_{\text{HM}} - T_{c, \text{HM}}) - c_{p_{\text{HM}}} T_0 \ln \left(\frac{T_{\text{HM}}}{T_{c, \text{HM}}} \right) \right)$	(6)
Chemical exergy of hot metal (MJ)	$E_{x, \text{ch, HM}} = \sum x_{\text{HM}, i} E_{x, \text{ch, HM}, i}$	(7)
Physical exergy of slag (MJ)	$E_{x, \text{ph, slag}} = m_{\text{slag}} \left(c_{p_{\text{slag}}} (T_{\text{slag}} - T_{c, \text{slag}}) - c_{p_{\text{slag}}} T_0 \ln \left(\frac{T_{\text{slag}}}{T_{c, \text{slag}}} \right) \right) + m_{\text{slag}} \Delta H \left(1 - \frac{T_{\text{slag}}}{T_{c, \text{slag}}} \right)$	(8)
Chemical exergy of slag (MJ)	$E_{x, \text{ch, slag}} = \sum x_{\text{slag}, i} E_{x, \text{ch, slag}, i}$	(9)
Physical exergy of dry gas (MJ)	$E_{x, \text{ph, D gas}} = m_{\text{D gas}} \left(c_{p_{\text{D gas}}} (T_{\text{D gas}} - T_0) - c_{p_{\text{D gas}}} T_0 \ln \left(\frac{T_{\text{D gas}}}{T_0} \right) \right) + \frac{1}{2} m_{\text{D gas}} v_{\text{D gas}}^2 + n_{\text{D gas}} R_0 T_0 \ln \left(\frac{p_{\text{D gas}}}{p_0} \right) \times 10^{-3}$	(10)
Chemical exergy of dry gas (MJ)	$E_{x, \text{ch, D gas}} = \sum x_{\text{D gas}, i} E_{x, \text{ch, D gas}, i} + R_0 T_0 \sum x_{\text{D gas}, i} \ln(x_{\text{D gas}, i})$	(11)
Physical exergy of water in gas (MJ)	$E_{x, \text{ph, w}} = m_{x, \text{ph, w}} \left(c_{p_w} (T_w - T_{c, w}) - c_{p_w} T_0 \ln \left(\frac{T_w}{T_{c, w}} \right) \right)$	(12)
Chemical exergy of water in gas (MJ)	$E_{x, \text{ch, w}} = x_{x, \text{ch, w}, i} E_{x, \text{ch, w}, i} + R_0 T_0 x_{x, \text{ch, w}, i} \ln(x_{x, \text{ch, w}, i})$	(13)
Exergy loss of chemical reaction (MJ)	$E_{x_l, r} = T_0 \Delta S_r \xi_r \times 10^{-3}$	(14)
Exergy loss during heat transfer (MJ)	$E_{x_l, \text{trans}} = T_0 Q_{\text{trans}} \left(\frac{1}{T_L} - \frac{1}{T_H} \right)$	(15)
Exergy loss of pressure and mixing process (MJ)	$E_{x_l, p \& m} = -R_0 T_0 \sum x_{p \& m, i} \ln(x_{p \& m, i}) + \frac{R_0 T_0 \ln \left(\frac{p_{\text{furnace hearth}}}{p_{\text{top}}} \right)}{22.4} \cdot \frac{V_{\text{blast}}}{1000}$	(16)
Exergy efficiency (%)	$\eta = \frac{E_{x, \text{ph, HM}} + E_{x, \text{ch, HM}} + E_{x, \text{ph, slag}} + E_{x, \text{ch, slag}}}{E_{\text{total}}} \times 100\%$	(17)

Table 3. Definition of symbols contained in Table 2.

Variable	Definition	Unit
$E_{x, ch, i}$	Chemical exergy of i ($i = \text{fuel, blast, iron ore, flux, hot metal (HM), slag, dry gas, and water in gas}$)	MJ
$E_{x, ph, i}$	Physical exergy of i ($i = \text{fuel, blast, iron ore, flux, hot metal (HM), slag, dry gas, and water in gas}$)	MJ
$E_{x, ch, i, j}$	Chemical exergy of each component (j) in i ($i = \text{blast, iron ore, flux, hot metal (HM), slag, dry gas, and water in gas}$) ($j = \text{each component in } i$)	MJ
$x_{i, j}$	Molar composition of each component (j) in i ($i = \text{blast, iron ore, flux, hot metal (HM), slag, dry gas, and water in gas}$) ($j = \text{each component in } i$)	%
V_g	Volume of gas	m^3
c_{pi}	Specific heat capacity of i ($i = \text{blast, hot metal, slag, dry gas, and water in gas}$)	$\text{MJ} \cdot \text{kg}^{-1} \cdot \text{K}^{-1}$
T_i	Temperature of i ($i = \text{blast, hot metal, slag, dry gas, and water in gas}$)	K
T_0	Temperature of reference state	K
p_0	Pressure of reference state	Pa
$T_{c, i}$	Phase transition temperature of i ($i = \text{hot metal, slag, and water in gas}$)	K
m_i	Mass of i ($i = \text{blast, hot metal, slag, fuel, dry gas, and water in gas}$)	kg
v_i	Velocity of i ($i = \text{blast and gas}$)	$\text{m} \cdot \text{s}^{-1}$
n_i	Mole of i ($i = \text{blast and dry gas}$)	mol
p_i	Pressure of gas i ($i = \text{blast, dry gas; position: furnace top and hearth}$)	Pa
Q_{low}	Standard low calorific value of fuel	$\text{MJ} \cdot \text{kg}^{-1}$
w	Mass fraction of water in fuel	%
r	Gasification latent heat of water: the heat for water to change from a liquid to a gaseous state	$\text{MJ} \cdot \text{kg}^{-1}$
ΔH	Melting heat during slag melting	$\text{MJ} \cdot \text{kg}^{-1}$
ΔS	Entropy changes of chemical reaction	$\text{kJ} \cdot \text{mol}^{-1}$
ξ_i	The reaction limit of reaction i	mol
Q_{tans}	Heat Transfer Quantity	MJ
T_L	Low temperature	K
T_H	High temperature	K
E_{total}	Total exergy input	MJ
$E_{xl, i}$	Exergy loss of i ($i = \text{chemical reaction, heat transfer, pressure, and mixing process}$)	MJ
η	Exergy efficiency	%

2.2. Material Balance Calculation

Some assumptions are necessary before the calculation: (1) This study considered solely the primary chemical processes occurring in the blast furnace. (2) Raw materials and products, such as ore and flux, coke, and gas, were considered ideal mixtures. (3) The temperatures of the ore and flux and fuel were equal to the environmental temperature.

In this paper, only the main chemical reactions in the blast furnace smelting process are considered: indirect reduction reactions of iron oxides (the reducing agent is CO) and methane (CH_4) generation that occurred in the block zone; direct reduction reactions of iron oxides (the reducing agent is C) and carburizing reduction that occurred in the cohesive zone; direct reduction reactions of silicon (Si), phosphorus (P), and manganese (Mn) oxides (the reducing agent is C) and desulfurization reactions that occurred in the dropping zone; and the combustion reaction of carbon, which occurred in the tuyere zone.

When calculating the material balance, the main raw materials for blast furnace smelting include sinter, pellet, lump ore, coke, coal, and flux, and the main products of blast furnace smelting include molten iron, slag, gas, and a small amount of furnace dust.

At the same time, certain blast operation parameters are required during smelting. All the information on the above-mentioned process are listed in Tables A1–A5 of Appendix A at the end of this paper.

Table 4 shows the calculation conditions of the exergy model of the blast furnace used in this study. It includes the fuel ratio (coke ratio and coal ratio), blast conditions (blast pressure, blast humidity, and blast temperature), and furnace top conditions (temperature and pressure).

Table 4. Calculation conditions of the exergy model of a blast furnace.

Parameter	Calculation Conditions	
Fuel ratio *	Coke ratio	310 kg
	Coal ratio	180 kg
Blast	Pressure	0.4 MPa
	Humidity	1.55%
	Temperature	1373 K
Furnace top	Temperature	473.15 K
	Pressure	0.25 MPa

* The fuel ratio (coke ratio or coal ratio) is denoted as the mass ratio of fuel (coke and coal) to hot metal.

The calculation of the material balance constitutes the fundamental theoretical calculations of blast furnace smelting. Table 5 shows the variables required for optimization in this study, which are the ore (sinter, pellet, and lump ore), flux, fuel ratio (coke and coal), blast, gas, slag, and components of hot metals (Fe, S, Si, P, Mn and C).

Table 5. Variables required for optimization in this study.

Variable	Unit	Definition	Variable	Unit	Definition
x_1	kg	Consumption of sinter	x_9	%	Content of S in hot metal
x_2	kg	Consumption of pellet	x_{10}	%	Content of Si in hot metal
x_3	kg	Consumption of lump ore	x_{11}	%	Content of P in hot metal
x_4	kg	Consumption of coke	x_{12}	%	Content of Mn in hot metal
x_5	kg	Consumption of coal	x_{13}	%	Content of C in hot metal
x_6	m ³	Blast volume	x_{14}	kg	Quantity of slag
x_7	m ³	Gas volume	x_{15}	kg	Amount of flux A
x_8	%	Content of Fe in hot metal	x_{16}	kg	Amount of flux B

The range of changes in slag composition involved in this study was based on the on-site slag of a domestic steel enterprise in China and the possible range of changes. Among them, the range of $w(\text{MgO})/w(\text{Al}_2\text{O}_3)$ in slag is 0.45 to 0.55, the range of R in slag is 1.20 to 1.30, and the range of $w(\text{Al}_2\text{O}_3)$ in slag is 15% to 20%.

A typical material balance of the blast furnace was calculated based on the given conditions ($w(\text{MgO})/w(\text{Al}_2\text{O}_3) = 0.55$, $R = 1.30$, and $w(\text{Al}_2\text{O}_3) = 15\%$). In this study, the input items included ore, coke, coal, flux, and blast, and the output items included hot metal, slag, gas, and dust. The established material balance of the blast furnace is shown in Table 6. Due to the relative error ($\bar{\Delta}$) < 0.03% as shown in Equation (18), the established material balance is reasonable.

$$\bar{\Delta} = \frac{(m_{\text{Input}} - m_{\text{Output}})}{m_{\text{Input}}} \times 100\% = 0.03\% \quad (18)$$

Table 6. Material balance table.

Input			Output		
Parameter	Quantity (kg)	Percent (%)	Parameter	Quantity (kg)	Percent (%)
Ore	1825.82	47.34	Hot metal	1000.00	25.94
Coke	338.46	8.78	Slag	518.47	13.44
Coal	180.00	4.67	Gas	2307.30	59.84
Flux	198.40	5.14	Dust	29.90	0.78
Blast	1314.24	34.07	Σ	3855.67	100.00
Σ	3856.92	100.00			

2.3. Exergy Balance Calculation

Figure 2 shows the exergy balance of the blast furnace smelting process, which consists of an exergy input item and an exergy output item. As shown in Figure 2, the process loss and external exergy loss of the blast furnace account for 71.71% of E_{total} , which is a significant percentage. Furthermore, the internal exergy loss accounted for 22.41% (31.25% of the total exergy loss) of the entire exergy output, while the external exergy loss accounted for 49.30% (68.75% of the total exergy loss) of the entire exergy output. Therefore, it is necessary to consider how to decrease the exergy loss of blast furnaces and increase their exergy efficiency. As shown in Figure 2, because the exergy of gas accounts for 30% of the total exergy, there is great significance for the utilization of gas.

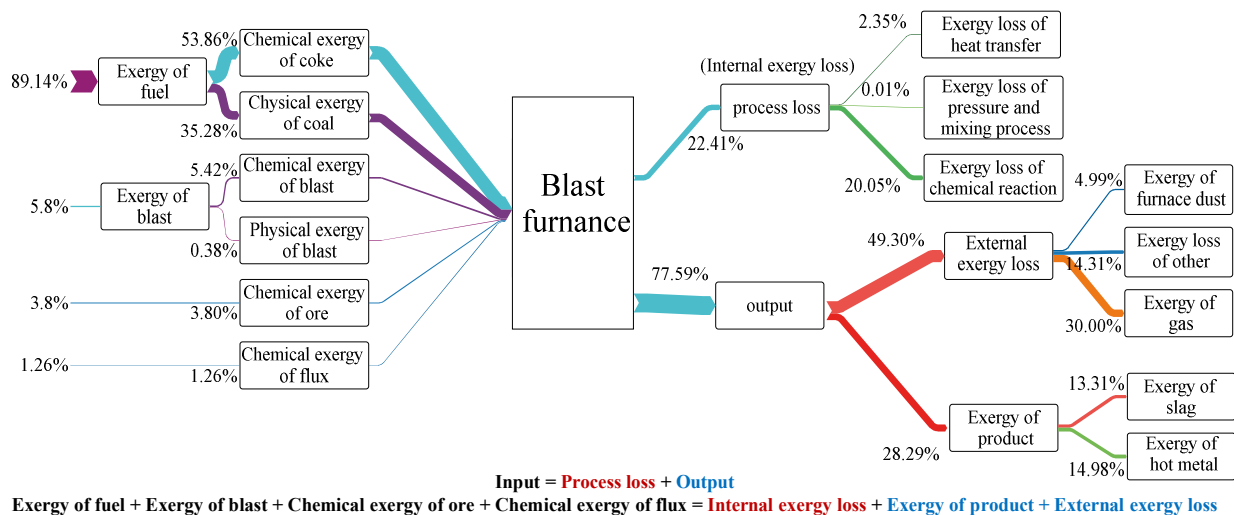


Figure 2. Exergy flows of the whole blast furnace.

3. Result and Discussion

The composition of blast furnace slag was evaluated based on the gray box exergy analysis model by discussing the influence of blast furnace slag compositions, including R , $w(\text{MgO})/w(\text{Al}_2\text{O}_3)$ and $w(\text{Al}_2\text{O}_3)$, on the blast furnace exergy efficiency (η). In addition, an objective function for minimizing the total exergy loss was developed, and its feasibility was verified by comparing the results of the objective function, gray box model, and actual production data.

3.1. Analysis of Blast Furnace Slag Composition Based on Exergy Analysis

Based on the gray box exergy analysis model, the influence of the blast furnace slag components R , $w(\text{MgO})/w(\text{Al}_2\text{O}_3)$ and $w(\text{Al}_2\text{O}_3)$ on the blast furnace exergy efficiency (η) was explored.

3.1.1. Effect of R on Exergy Efficiency (η)

According to the established gray box exergy analysis model, the effect of R on the η of the blast furnace is obtained in Figure 3. As shown in Figure 3a, the η of the blast furnace smelting process exhibited a slightly upward tendency with an increase in R when $w(\text{Al}_2\text{O}_3) = 15\%$. Nevertheless, Figure 3b,c show that there was no discernible change in η with an increase in R when $w(\text{Al}_2\text{O}_3) = 18\%$ or 20% . As shown in Figure 3, when $w(\text{MgO})/w(\text{Al}_2\text{O}_3)$ is constant, η gradually decreases as $w(\text{Al}_2\text{O}_3)$ increases from 15% to 20% . The reason for this phenomenon was that when $w(\text{Al}_2\text{O}_3) = 15\%$, $E_{x, \text{ph, slag}}$ and $E_{x, \text{ch, slag}}$ exhibited a slightly upward tendency (Figure 4a), but there was no discernible change in $E_{x, \text{ph, slag}}$ and $E_{x, \text{ch, slag}}$ with an increase in R when $w(\text{Al}_2\text{O}_3) = 18\%$ or 20% (Figure 4b,c). Based on Equation (17), there was a positive correlation between $E_{x, \text{ch, slag}}$ and η . Therefore, the results in Figure 4 were obtained. On the other hand, as shown in Figure 4a, when $w(\text{Al}_2\text{O}_3) = 15\%$, the relative slope ($k = ((y_2 - y_1) \cdot y_1) / ((x_2 - x_1) \cdot x_1)$, x : The abscissa of a point, y : The vertical axis of a point) of the change curve for $E_{x, \text{ph, slag}}$ and $E_{x, \text{ch, slag}}$ was $k_{x, \text{ph, slag}} = 1.68$ and $k_{x, \text{ch, slag}} = 0.8$, which was higher than the k for $E_{x, \text{ph, slag}}$ and $E_{x, \text{ch, slag}}$ when $w(\text{Al}_2\text{O}_3) = 18\%$ and 20% (Figure 4b,c). As a result of k , the η of the blast furnace smelting process exhibited a slightly upward tendency with an increase in R when $w(\text{Al}_2\text{O}_3) = 15\%$, but there was no discernible change in η with an increase in R when $w(\text{Al}_2\text{O}_3) = 18\%$ or 20% .

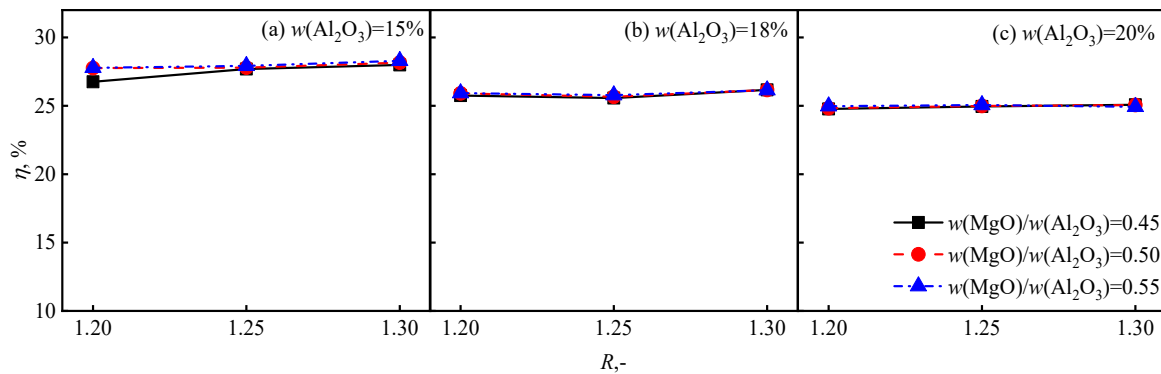


Figure 3. Effect of R on η .

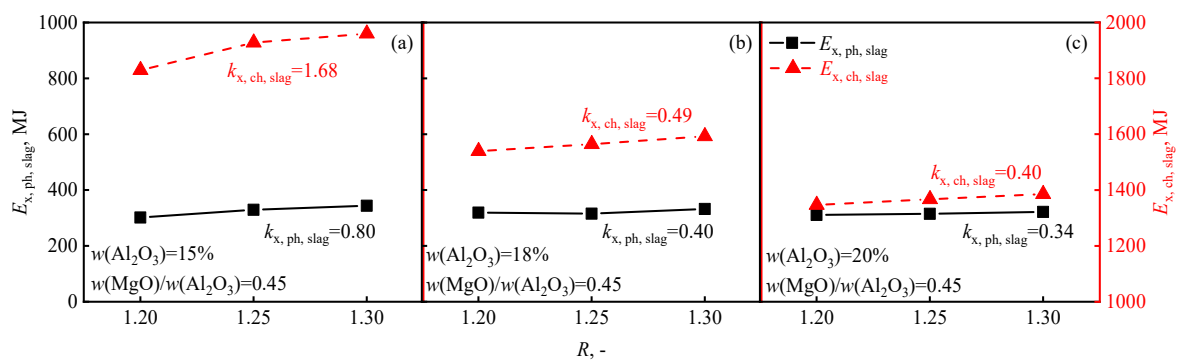


Figure 4. Effect of R on $E_{x, \text{ph, slag}}$ and $E_{x, \text{ch, slag}}$.

3.1.2. Effect of $w(\text{MgO})/w(\text{Al}_2\text{O}_3)$ on Exergy Efficiency (η)

The effect of $w(\text{MgO})/w(\text{Al}_2\text{O}_3)$ on the η of the blast furnace is shown in Figure 5. As shown in Figure 5a, with the increase in $w(\text{MgO})/w(\text{Al}_2\text{O}_3)$, the η of the blast furnace shows a slight upward trend at $w(\text{Al}_2\text{O}_3) = 15\%$. However, Figure 5b,c show that there is no discernible change at $w(\text{Al}_2\text{O}_3) = 18\%$ or 20% . As shown in Figure 5, $w(\text{MgO})/w(\text{Al}_2\text{O}_3)$ is constant when $w(\text{Al}_2\text{O}_3) = 15\%$, and as R increases from 1.20 to 1.25 , η increases, and R increases from 1.25 to 1.30 , while η shows no discernible change. When $w(\text{Al}_2\text{O}_3) = 18\%$

and 20%, with the increase in R , η shows no discernible change. The reason for this change was that when $w(\text{MgO})/w(\text{Al}_2\text{O}_3)$ decreases from 0.45 to 0.25, the viscosity of the slag increases from 0.32 Pa·s to 0.35 Pa·s under the condition of $w(\text{Al}_2\text{O}_3) < 15\%$; when $w(\text{MgO})/w(\text{Al}_2\text{O}_3)$ decreases from 0.45 to 0.25, the viscosity of the slag increases from 0.32 Pa·s to 0.48 Pa·s under the condition of $w(\text{Al}_2\text{O}_3) > 18\%$ [30]. Therefore, the increase in $w(\text{MgO})/w(\text{Al}_2\text{O}_3)$ will lead to a decrease in the viscosity of the blast furnace slag, which is beneficial for the smooth operation of the blast furnace, reducing the energy consumption during the smelting process and indirectly improving the exergy efficiency of the blast furnace smelting process. In addition, with the increase in $w(\text{MgO})/w(\text{Al}_2\text{O}_3)$, the total exergy (E_{total}) of the blast furnace underwent no discernible change, while the exergy of the slag ($E_{x, \text{slag}} = E_{x, \text{ph, slag}} + E_{x, \text{ch, slag}}$) gradually increased, as shown in Figure 6a. As shown in Figure 6b,c, when $w(\text{Al}_2\text{O}_3) = 18\%$ or 20%, E_{total} and $E_{x, \text{slag}}$ underwent no discernible change. The relative slope ($k_{x, \text{slag}}$) of the change curve in $E_{x, \text{slag}}$ was greater than the relative slope (k_{total}) of the change curve in E_{total} , and based on Equation (17), η increased. However, as shown in Figure 6b,c, when $w(\text{Al}_2\text{O}_3) = 18\%$ or 20%, there was no discernible change in η with an increase in $w(\text{MgO})/w(\text{Al}_2\text{O}_3)$ due to the low k .

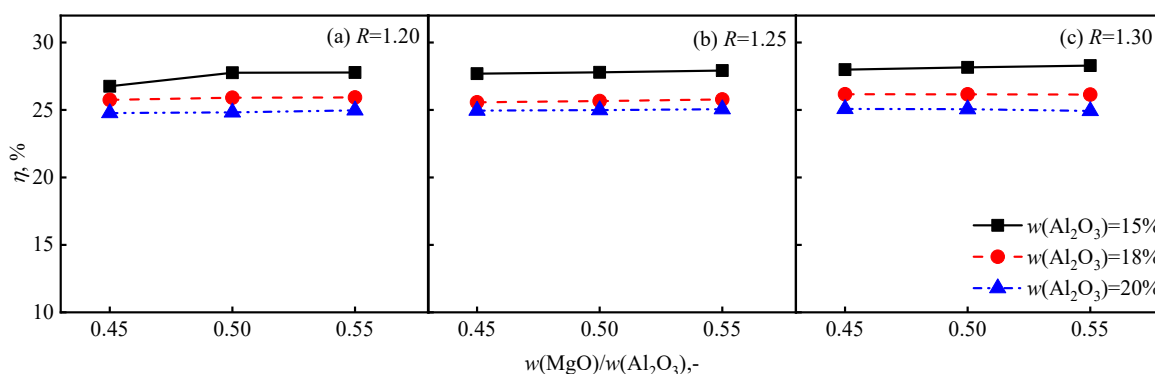


Figure 5. Effect of $w(\text{MgO})/w(\text{Al}_2\text{O}_3)$ on η .

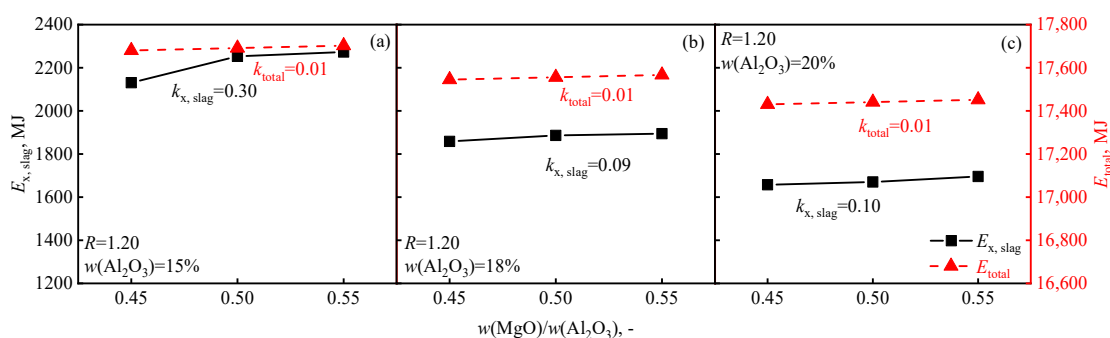


Figure 6. Effect of $w(\text{MgO})/w(\text{Al}_2\text{O}_3)$ on $E_{x, \text{slag}}$ and E_{total} .

3.1.3. Effect of $w(\text{Al}_2\text{O}_3)$ on Exergy Efficiency (η)

Figure 7 shows the effect of $w(\text{Al}_2\text{O}_3)$ on the η of the blast furnace. As shown in Figure 7, the η of blast furnace slag decreased as $w(\text{Al}_2\text{O}_3)$ increased from 15% to 20%. The reason was that when $R = 1.15$, $w(\text{MgO})/w(\text{Al}_2\text{O}_3) = 0.25$, $w(\text{Al}_2\text{O}_3)$ increased from 15% to 18%, and the slag viscosity increased from 0.37 to 0.45. When $R = 1.15$, $w(\text{MgO})/w(\text{Al}_2\text{O}_3) = 0.35$, $w(\text{Al}_2\text{O}_3)$ increased from 15% to 18%, and the slag viscosity increased from 0.37 to 0.42. When $R = 1.15$, $w(\text{MgO})/w(\text{Al}_2\text{O}_3) = 0.45$, $w(\text{Al}_2\text{O}_3)$ increased from 15% to 18%, and the slag viscosity increased from 0.26 to 0.36 [31]. Therefore, the increase in $w(\text{Al}_2\text{O}_3)$ led to an increase in slag viscosity, hindered the smooth operation of the blast furnace, and the exergy of gas ($E_{x, \text{gas}} = E_{x, \text{ph, D gas}} + E_{x, \text{ch, D gas}} + E_{x, \text{ph, w}} + E_{x, \text{ch, w}}$) decreased, which led to an increase in the external exergy loss ($E_{x\text{l, ex}}$) of the blast furnace. On the

other hand, with the increase in the $w(\text{Al}_2\text{O}_3)$ content of the blast furnace slag, the exergy of the slag ($E_{x, \text{slag}} = E_{x, \text{ph, slag}} + E_{x, \text{ch, slag}}$) decreased; according to Equation (17), the η of the blast furnace decreased. Thus, the exergy efficiency of the blast furnace decreased with increasing $w(\text{Al}_2\text{O}_3)$. $E_{x, \text{slag}}$ and $E_{x, \text{gas}}$ decreased with increasing $w(\text{Al}_2\text{O}_3)$, while $E_{\text{xl, ex}}$ increased with increasing $w(\text{Al}_2\text{O}_3)$, as shown in Figure 8. This is because that with the increase in $w(\text{Al}_2\text{O}_3)$, $E_{\text{xl, ex}}$ increases, resulting in an increase in the blast furnace exergy loss (E_{xl}) and a decrease in the exergy efficiency (η). On the other hand, according to Equation (17), $E_{x, \text{slag}}$ is positively correlated with η , so the decrease in $E_{x, \text{slag}}$ will lead to a decrease in η . Therefore, as shown in Figure 7, with the increase in $w(\text{Al}_2\text{O}_3)$, η decreases.

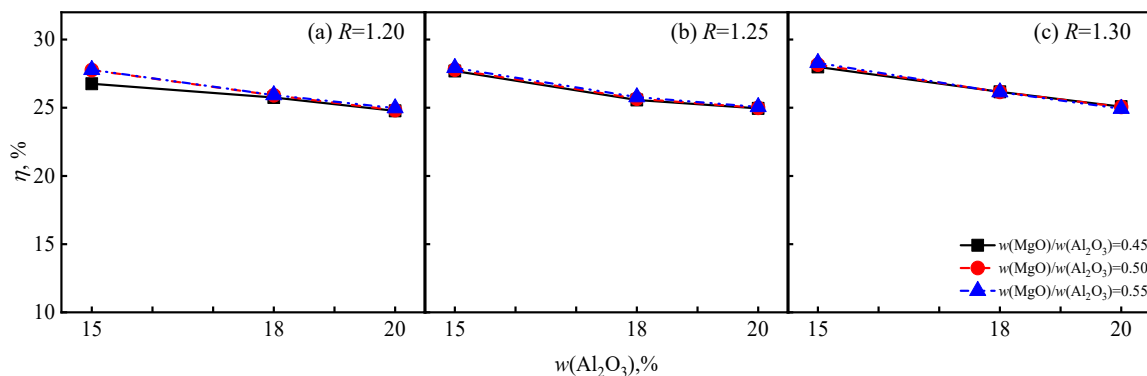


Figure 7. Effect of $w(\text{Al}_2\text{O}_3)$ on η .

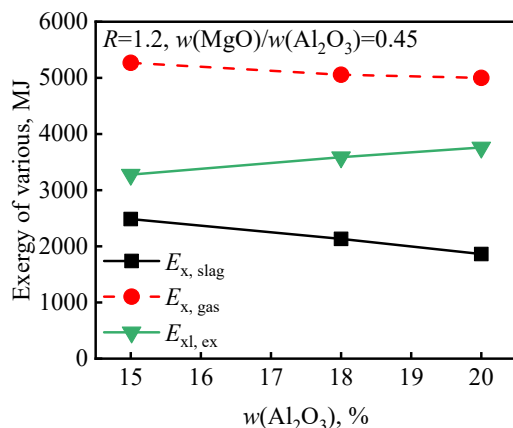


Figure 8. Effect of $w(\text{Al}_2\text{O}_3)$ on $E_{x, \text{slag}}$, $E_{x, \text{gas}}$, and $E_{\text{xl, ex}}$: $R = 1.20$ and $w(\text{MgO})/w(\text{Al}_2\text{O}_3) = 0.45$.

Based on the above results, the η of the blast furnace smelting process was 28.29%, and the minimal exergy loss ($E_{\text{xl, min}}$) was 7395.45 MJ with slag compositions of $R = 1.30$, $w(\text{MgO})/w(\text{Al}_2\text{O}_3) = 0.55$, and $w(\text{Al}_2\text{O}_3) = 15\%$.

3.2. Optimization of Blast Furnace Slag Composition Based on Exergy Analysis

In order to minimize the exergy loss and optimize the composition of the blast furnace slag, an objective function based on a gray box exergy analysis model of the blast furnace was constructed. This function was solved using LINGO, considering operating variables, constraints on product parameters, and balancing constraints.

3.2.1. Establishment of the Objective Function

Tables 7 and 8 are the constraints on the product composition and the balance constraints for establishing the objective function, including constraints on product parameters, respectively. The primary variables (ore, fuel ratio, blast volume, blast temperature, flux, quality criteria of hot metal, blast furnace gas, and slag) are listed in Table 5. Using the

above constraints and variables, an objective function of *min* was established by combining the nonlinear programming method and gray box exergy analysis model, which is shown in Equation (19).

$$\begin{aligned} \min = & 1.5x_1 + 0.168x_2 + 0.141x_3 + 0.176x_4 + 91.278x_5 + 0.007x_6 + 0.333x_7 + 2.012x_8 - \\ & 27.289x_9 + 154.8x_{10} + 229.9x_{11} + 39.0x_{12} + 60.36x_{13} + 1.188x_{14} + 0.889x_{15} + \\ & 0.872x_{16} - 0.25x_5^2 - 0.032x_5x_6 - 0.0024x_6x_7 - 0.016x_5x_7 + 0.0004x_7x_8 + 5269.86 \end{aligned} \quad (19)$$

Table 7. Constraints on product compositions.

Parameter	Definition	Constraint Condition
Product composition constraints	Constraints on hot metal composition	$x_8 + x_9 + x_{10} + x_{11} + x_{12} + x_{13} = 100$
	Constraints on Si content in hot metal	$x_{10} \geq 0.2$
	Constraints on coal injection volume	$120 \leq x_5 \leq 200$

Table 8. Material balancing constraints.

Parameter	Constraint Condition
R constraint	$\frac{0.0697x_1 + 0.0095x_2 + 0.003x_3 + 0.006x_4 + 0.0055x_5 + 0.5411x_{15}}{0.073x_1 + 0.0322x_2 + 0.1246x_3 + 0.0589x_4 + 0.0842x_5 - 21.4286x_{10} + 0.0077x_{15}} \in [1.20, 1.30]$
$w(\text{MgO})/w(\text{Al}_2\text{O}_3)$ constraint	$\frac{0.0099x_1 + 0.0089x_2 + 0.0032x_3 + 0.0015x_4 + 0.0015x_5 + 0.0118x_{15} + 0.5423x_{16}}{0.0543x_1 + 0.947x_2 + 0.0147x_3 + 0.0408x_4 + 0.0542x_5 + 0.0012x_{15} + 0.001x_{16}} \in [0.45, 0.55]$
$w(\text{Al}_2\text{O}_3)$ constraint	$0.0534x_1 + 0.947x_2 + 0.015x_3 + 0.0408x_4 + 0.054x_5 + 0.0012x_{15} + 0.001x_{16} \in [0.15x_{14}, 0.20x_{14}]$
Fe	$0.5580x_1 + 0.6509x_2 + 0.5788x_3 + 0.0091x_4 + 0.0088x_5 = 10.0246x_8$
C	$0.00011x_1 + 0.0000712x_2 + 0.00014x_3 + 0.465126x_4 + 0.4407x_5 - 0.96x_8 - 1.875x_9 + 8.57x_{10} + 2.1818x_{12} + 9.6774x_{11} + 10x_{13} + 0.218x_{15} + 0.2288x_{16} = 0.853x_4 + 0.8073x_5$
P	$10x_{11} = 0.0006x_1 + 0.0006x_2 + 0.0002x_3$
S	$10x_9 = 0.00006010x_1 + 0.00004007x_2 + 0.00008013x_3 + 0.0005409x_4 + 0.00015025x_5$
Mn	$10x_{12} = 0.00115x_1 + 0.001375x_2 + 0.0011761x_3 + 0.0023625x_4$
Slag balance constraint	$4x_{14} = 0.766785x_1 + 1.65154x_2 + 0.725232x_3 + 0.123728x_4 + 0.154902x_5 - 5x_9 - 21.4286x_{10} + 0.5618x_{15} + 0.5442x_{16}$
Blast balance constraint	$x_6 = 1.9260x_4 + 1.6518x_5$
Gas balance constraint	$x_7 = 0.0085x_1 - 0.0005x_2 + 0.0111x_3 + 0.8811x_4 + 0.8987x_5 + 0.7878x_6 + 1.8x_8 - 3.5x_9 + 15.9999x_{10} + 18.0645x_{11} + 4.0727x_{12} + 0.5184x_{15} + 0.5425x_{16}$
Material balance constraint	$1.03(x_1 + x_2 + x_3) + 1.1962x_4 + 1.068x_5 + 1.2941x_6 + 1.068x_{15} + 1.068x_{16} = 0.03x_1 + 0.03x_2 + 0.0405x_3 + 0.2167x_4 + 0.0632x_5 + 0.0062x_6 + 1.4068x_7 + x_{14} + 0.068x_{15} + 0.068x_{16} + 1000$

3.2.2. Solution of the Objective Function

The objective function was resolved by combining the established constraints with LINGO software (LINGO 18). The obtained optimal solution is 7129.42 MJ with a slag composition of $R = 1.295$, $w(\text{MgO})/w(\text{Al}_2\text{O}_3) = 0.545$, and $w(\text{Al}_2\text{O}_3) = 15\%$. It was demonstrated that the established objective function converges in the feasible domain because the infeasibility of the function was 1.84525×10^{-11} , which is close to zero. In other words, the calculation of the result by the objective function was logical.

3.2.3. Verification of the Objective Function

A data comparison of the objective function, gray box model, and actual production results [32] is shown in Figure 9.

Using the actual results as a benchmark, the accuracy of the results of the objective function and the gray box model was verified by comparing them with the structure of the objective function and the gray box model. As shown in Figure 9, the objective function was more accurate than the gray box exergy analysis model because the error between the

objective function and the actual results (1.2%) was lower than that between the model calculation results and the actual production results (2.4%). Based on comparison, it can be concluded that the objective function was more accurate than the gray box exergy analysis model. Therefore, the results of the objective function are relatively accurate over the range of this study and the objective function can be used for optimizing the blast furnace slag from the view of exergy efficiency.

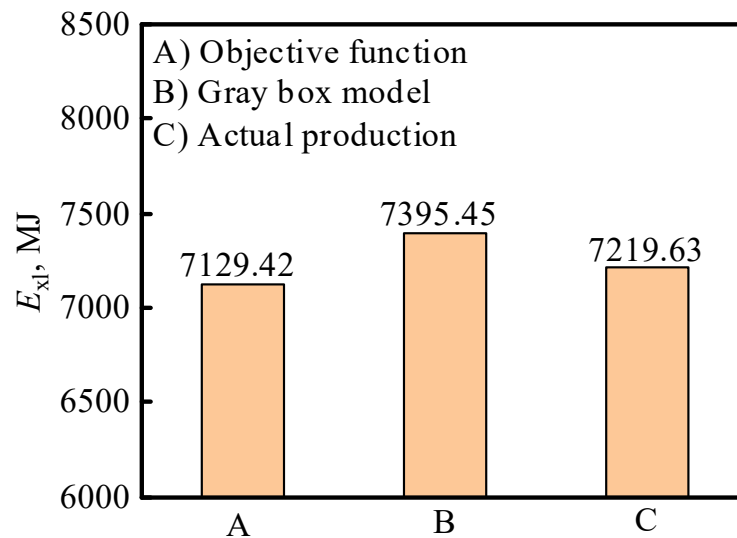


Figure 9. The objective function, gray box model, and actual production exergy loss are compared.

4. Conclusions

The objectives of exergy reduction and blast furnace consumption reduction can be accomplished by reducing energy loss and increasing η . For the smelting of a blast furnace, a gray box exergy analysis model was constructed. The effect of the composition of the blast furnace slag, including R , $w(\text{MgO})/w(\text{Al}_2\text{O}_3)$ and $w(\text{Al}_2\text{O}_3)$, on η was investigated. An objective function for the minimum exergy loss was established. The analysis results are as follows:

1. The total exergy loss of the blast furnace accounted for a relatively high proportion of the exergy expenditure, approximately 71.71% of E_{total} . Of this, the internal exergy loss ($E_{xl, \text{in}}$) accounted for 22.41% (31.25% of the total exergy loss) of E_{total} , while the external exergy loss ($E_{xl, \text{ex}}$) accounted for 49.30% (68.75% of the total exergy loss) of E_{total} . At the same time, because the exergy of the gas accounts for 30% of E_{total} , there is great significance for gas utilization.
2. Based on the established gray box exergy analysis model, when $w(\text{Al}_2\text{O}_3) = 15\%$, the exergy efficiency (η) of the blast furnace exhibited an upward trend with increasing slag R and $w(\text{MgO})/w(\text{Al}_2\text{O}_3)$. However, there was no discernible change in the exergy efficiency of the slag with an increase in R and $w(\text{MgO})/w(\text{Al}_2\text{O}_3)$ when $w(\text{Al}_2\text{O}_3) = 18\%$ or 20% . The exergy efficiency (η) of the blast furnace decreased with increasing $w(\text{Al}_2\text{O}_3)$. The exergy efficiency (η) of the blast furnace smelting process was 28.29%, and the minimal exergy loss ($E_{xl, \text{min}}$) was 7395.45 MJ with slag compositions of $R = 1.30$, $w(\text{MgO})/w(\text{Al}_2\text{O}_3) = 0.55$, and $w(\text{Al}_2\text{O}_3) = 15\%$.
3. An objective function based on the gray box exergy analysis model of the blast furnace was constructed and solved using LINGO. For the calculation, the calculation of the result with the objective function was logical. The obtained optimal solution was 7129.42 MJ with a slag composition of $R = 1.295$, $w(\text{MgO})/w(\text{Al}_2\text{O}_3) = 0.545$, and $w(\text{Al}_2\text{O}_3) = 15\%$. The calculation results of the model and the objective function are compared with the actual production results, respectively. Because the error between the objective function and the actual result (1.2%) is lower than the error between

the model calculation result and the actual result (2.4%), the result of the objective function is more accurate within the experimental range.

Author Contributions: Conceptualization, Z.W. and H.Z.; methodology, Z.W.; software, Z.W. and H.Z.; validation H.Z., Y.Z. and L.G.; formal analysis, Z.W.; investigation, Z.W. and Y.Z.; resources, H.Z.; data curation, Z.W.; writing—original draft preparation, Z.W.; writing—review and editing Z.W., H.Z., Y.Z., and L.G.; visualization, Z.W. and H.Z.; project administration, H.Z.; funding acquisition, H.Z. All authors have read and agreed to the published version of the manuscript.

Funding: Financial support from the National Natural Science Foundation of China (NSFC52074072, NSFC51774071) under grants is gratefully acknowledged.

Data Availability Statement: The original contributions presented in the study are included in the article, and further inquiries can be directed to the corresponding authors.

Acknowledgments: The authors are grateful to X.J. (Xin Jiang), Q.G. (Qiangjian Gao), and F.S. (Fengman Shen) at the Northeastern University of China for valuable discussions and suggestions throughout this study.

Conflicts of Interest: The authors declare that they have no known competing financial interests or personal relationships that could have appeared to influence the work reported in this paper.

Appendix A

Table A1. Compositions of iron-bearing materials for blast furnace smelting, %.

	TFe *	FeO	SiO ₂	Al ₂ O ₃	CaO	MgO	MnO	FeS	P ₂ O ₅	H ₂ O	CO ₂
Sinter	51.45	18.18	7.76	3.00	13.70	3.74	0.12	0.09	0.11	0.00	0.00
Pellet	63.88	4.11	3.50	2.80	2.50	0.04	0.16	0.11	0.08	0.00	0.00
Lump ore	48.57	6.20	10.84	2.32	2.12	0.40	0.16	0.00	0.05	6.110	9.30

* TFe: The total content of iron element determined by chemical analysis of the ore.

Table A2. Composition of coke, %.

C	Ash Content							Volatile Matter					Organic Matter			Free Water, %	
	SiO ₂	Al ₂ O ₃	CaO	MgO	FeO	FeS	MnO	CO ₂	CO	CH ₄	H ₂	N ₂	H ₂	N ₂	S		Σ
84.46	6.36	5.42	0.87	0.12	0.85	0.03	0.01	0.26	0.27	0.03	0.04	0.14	0.3	0.3	0.54	100	5.66

Table A3. Composition of coal, %.

C	H	O	N	S	H ₂ O	SiO ₂	Al ₂ O ₃	CaO	MgO	FeO	Σ
75.3	3.26	3.16	0.34	0.36	0.8	9.39	5.82	0.2	0.16	1.21	100

Table A4. Composition of flux, %.

	TFe	FeO	SiO ₂	Al ₂ O ₃	CaO	MgO	MnO	FeS	P ₂ O ₅	H ₂ O	CO ₂
flux	0.00	0.00	0.00	0.13	54.11	1.16	0.00	0.07	0.01	0.00	43.79

Table A5. Element distribution ratio.

	Fe	Mn	P	S
Hot metal	0.9975	0.5	1	
Slag	0.0025	0.5	0	
Gas	0	0	0	0.05

References

1. Yu, J.Y.; Xu, R.S.; Zhang, J.L.; Zheng, A.Y. A review on reduction technology of air pollutant in current China's iron and steel industry. *J. Clean.* **2023**, *414*, 137659. [[CrossRef](#)]
2. Li, Z.X.; Andersson, F.N.G.; Nilsson, L.J.; Åhman, M. Steel decarbonization in China—A top-down optimization model for exploring the first steps. *J. Clean.* **2023**, *384*, 135550. [[CrossRef](#)]
3. Wang, G.; Xue, G.Q.; Wang, S.J. Effect of mixing charge of highly reactive semicoke nut on the reaction of high Al₂O₃ ferrous burden in blast furnace. *Ironmak. Steelmak.* **2019**, *46*, 477–484. [[CrossRef](#)]
4. Talapaneni, T.; Yedla, N.; Sarkar, S. Study on desulfurization capacity of high alumina blast furnace slag at 1773K using slag–metal equilibrium technique. *Metall. Res. Technol.* **2018**, *115*, 8. [[CrossRef](#)]
5. Wang, C.L.; Lu, Q.; Zhang, S.H.; Li, F.M. Study on sulphide capacity of CaO–SiO₂–Al₂O₃–MgO–Fe₂O slags. *J. Univ. Sci. Technol. Beijing Miner. Met. Mater.* **2006**, *13*, 213–217. [[CrossRef](#)]
6. Wu, S.L.; Lu, Y.N.; Hong, Z.B.; Zhou, H. Improving the Softening and Melting Properties of Ferrous Burden with High Al₂O₃ Content for Blast Furnace by Ore Blending. *ISIJ Int.* **2020**, *60*, 1504–1511. [[CrossRef](#)]
7. Pang, Z.D.; Lv, X.W.; Ling, J.W.; Jiang, Y.Y.; Yan, Z.M.; Dang, J. Blast Furnace Ironmaking Process with Super–High TiO₂ in the Slag: Sulfide Capacity. *Metall. Mater. Trans. B* **2021**, *29*, 1170–1178. [[CrossRef](#)]
8. Trinath, T.; Vatsala, C. Proposing a suitable slag composition by estimating the fusion behavior, viscosity and desulfurization ability for blast furnaces running with high alumina. *Mater. Today Proc.* **2022**, *67*, 558–565. [[CrossRef](#)]
9. Lu, Y.; Ren, S.; Wang, X.Q.; Dong, L.Y.; Yang, J.F.; Liu, J.B. Effect of Al₂O₃, MgO and CaO/SiO₂ on Viscosity of High Alumina Blast Furnace Slag. *Steel Res. Int.* **2016**, *87*, 241–249. [[CrossRef](#)]
10. Wang, S.; Jiang, Y.; Guo, Y.F.; Yang, Z.; Chen, F.; Yang, L.Z.; Li, G. Effects of Basicity and Al₂O₃ Content on Viscosity and Crystallization Behavior of Super-High-Alumina Slag. *Crystals* **2022**, *12*, 851. [[CrossRef](#)]
11. Kim, H.; Wan, H.K.; Sohn, I.; Dong, J.M. The Effect of MgO on the Viscosity of the CaO–SiO₂–20wt%Al₂O₃–MgO Slag System. *Steel Res. Int.* **2010**, *81*, 261–264. [[CrossRef](#)]
12. Lv, X.W.; Yan, Z.M.; Pang, Z.D.; Bai, C.G.; Liang, D.; Xie, H. Effect of Al₂O₃ on physicochemical properties and structure of blast furnace slag: Reviewed. *Iron Steel* **2020**, *55*, 1–10. [[CrossRef](#)]
13. Shen, F.M. Discussion on the smelting process of high Al₂O₃ content slag-based blast furnace. *Angang Technol.* **2005**, *6*, 1–4.
14. Zheng, H.Z.; Liang, L.S.; Du, J.L.; Zhou, S.F.; Jiang, X.; Gao, Q.J.; Shen, F.M. Mineral Transform and Specific Heat Capacity Characterization of Blast Furnace Slag with High Al₂O₃ in Heating Process. *Steel Res. Int.* **2020**, *92*, 2000448. [[CrossRef](#)]
15. Hu, A.G. China's goal of achieving carbon peak by 2030 and its main approaches. *J. Beijing Tech. Univ. Soc. Sci.* **2021**, *21*, 1–15.
16. Liu, Z.J.; Wang, J.B.; Zhang, J.L.; Wang, Y.Z.; Niu, L.L.; Zhu, W. Status of energy consumption and prospect of consumption reduction technology in blast furnace. *J. Iron. Steel Res.* **2023**, *35*, 1–10.
17. Wang, X.D.; Qie, Y.N.; Lv, Q.; Wang, Y.F. Analysis and comparison of energy saving and emission reduction of blast furnace injection with different hydrogen-rich mediums. *Iron Steel* **2023**, *58*, 34–41.
18. Szargut, J. Exergetic balance of metallurgical processes. *Arch. Hut.* **1961**, *6*, 23–60.
19. Brauer, H.; Jeschar, R. The significance of exergy for the thermodynamic study of the blast-furnace process. *Arch. Eisenhuettenwesen* **1963**, *34*, 9–16.
20. Akiyama, T.; Yagi, J.I. Exergy analysis of conventional ironmaking, direct reduction–electric furnace and smelting reduction systems. *Tetsu Hagane* **1988**, *74*, 2270–2277. [[CrossRef](#)]
21. Akiyama, T. Preface to the “Special Issue on Science and Technologies for the Effective Use of Unrecovered Energy in Steelworks”. *ISIJ Int.* **2010**, *50*, 1221–1228. [[CrossRef](#)]
22. Akiyama, T.; Takahashi, R.; Yagi, J.I. Exergy evaluation on the pellets production and direct reduction processes for the fired and cement bonded pellets. *Tetsu Hagane* **1987**, *73*, 2108–2115. [[CrossRef](#)] [[PubMed](#)]
23. Liu, G.G.; Li, L.; Li, Z.J.; Fan, H.; Qin, J.; Qi, J.L. Exergy analysis of a 240 t/h gas fired boiler in a panzhihua steel company: Energy and thermal engineering branch of China metal society. In Proceedings of the 10th National Annual Conference on Energy and Thermal Engineering Energy and Thermal Engineering Branch of China Metal Society, Northeast University, Energy and Thermal Engineering Branch of China Metal Society, Dalian, China, 8–10 July 2019; pp. 170–176.
24. Min, Y.; Zhang, Q.; Jiang, M.F.; Huang, J.; Zhang, D. Exergy analysis of LF refining process. *Ind. Heat.* **2008**, *37*, 49.
25. Wang, Y.; Zhao, X.; Xu, J.; Zhang, Q. Energy and exergy analyses of an integrated iron and steel making process. *Int. J. Exergy* **2018**, *26*, 454. [[CrossRef](#)]
26. Guo, J.; Chu, M.S.; Tang, J.; Li, F.; Liu, Z.G.; Bao, J.W. Exergy Analysis of Iron Coke Used in Blast Furnace. *Iron Steel* **2022**, *57*, 30–38.
27. Qiu, Z.Y.; Yue, Q.; Yan, T.Y.; Wang, Q.; Sun, J.C.; Yuan, Y.X.; Che, Z.C.; Wang, Y.S.; Du, T. Gas utilization optimization and exergy analysis of hydrogen metallurgical shaft furnace. *Energy* **2023**, *263*, 125847. [[CrossRef](#)]
28. Sun, J.C.; Na, H.M.; Yan, T.Y.; Qiu, Z.Y.; Yuan, Y.X.; He, J.F.; Li, Y.N.; Wang, Y.S.; Du, T. A comprehensive assessment on material, exergy and emission networks for the integrated iron and steel industry. *Energy* **2021**, *235*, 121429. [[CrossRef](#)]
29. GB/T14909-2021; Technical Guidelines for Exergy Analysis in Energy Systems. National Energy Foundation and Management Standardization Technical Committee: Washington, DC, USA, 2021.
30. Shen, F.M.; Jiang, X.; Gao, Q.J.; Zheng, H.Y. Theoretical Basis for Suitable Magnesium Aluminum Ratio of Blast Furnace Slag. *Ironmaking* **2019**, *38*, 17–21.

31. Hu, Y.P. Effect of Al_2O_3 on Metallurgical Properties of Blast Furnace Slag and Viscosity Prediction Model. Master's Thesis, Northeast University, Shenyang, China, 2017.
32. Guo, T.L. Basic Research on a New Low Carbon Iron Making Process by Injecting Coke Oven Gas into Blast Furnace. Ph.D. Thesis, Northeast University, Shenyang, China, 2015.

Disclaimer/Publisher's Note: The statements, opinions and data contained in all publications are solely those of the individual author(s) and contributor(s) and not of MDPI and/or the editor(s). MDPI and/or the editor(s) disclaim responsibility for any injury to people or property resulting from any ideas, methods, instructions or products referred to in the content.